Earthquake Geotechnical Engineering for Protection and Development of Environment and Constructions – Silvestri & Moraci (Eds)
© 2019 Associazione Geotecnica Italiana, Rome, Italy, ISBN 978-0-367-14328-2

Shaking table test on the asynchronous responses of the shaft-tunnel junction under transverse excitations

J. Zhang & Y. Yuan
Tongji University, Shanghai, China

ABSTRACT: Due to the special configurations of the shaft-tunnel junction, the asynchronous responses of the shaft and the tunnel will arise when earthquakes strike. This paper presents the design and conclusions of a shaking table test addressing this phenomenon. The model scale is 1:60. A synthetic soil composed of sawdust and sand is developed to match the degradation curves of the actual ground soil. Segmental equivalent rings are designed to form up the tunnel model. The shaft model is fabricated by 3D-print technology. It reveals that the shaft model is more sensitive to earthquake accelerations in the range of 10 Hz to 30 Hz. The discrepancy is quantified by correlation coefficients of acceleration time histories. The asynchronous responses have caused significant increase in extensions of circumferential joints at the shaft-tunnel junction.

1 INTRODUCTION

1.1 *Asynchronous responses*

A special issue regarding the seismic analysis of extended structures is the asynchronous responses among different structural components. One cause for that is the non-uniform earthquake excitations. (Kiureghian, 1996) Another one would be the variations of structural stiffness. In the case of long tunnels, the structure is not always spatially uniform. Constructions of vertical shafts and transverse passages would cause a sharp change of structural stiffness. Even under uniform excitations, these 'non-uniform parts' tend to behave asynchronously, so they are more likely to suffer from seismic damages. (Koizumi, 2009)

1.2 *Shaft-tunnel junction*

Because of the special techniques of shield tunneling method, shield-driven tunnels in soft soils are often constructed with vertical shafts. The shield machine could initiate or terminate a tunnel zone after leaving of entering a vertical shaft. Shafts could also serve as the transition point between surface and underground spaces during the operating period. Unlike the tunnel lining, which is segmental and lengthy, vertical shafts are much stiffer and have comparatively limited dimensions. Although the shaft and the tunnel could be positioned in similar ground conditions under the same dynamic loading, they tend to behave asynchronously due to the distinctive structural differences. The prototype structure for the shaking table test is a newly built shield- driven tunnel used for highway transportation in the city of Shanghai. The vertical shaft alone is 55.0 m long, 26.8 m wide and 23.3 m high. The diameter of the tunnel is 15.0 m. As the consequence of complicated construction procedures, the structural properties of the shaft-tunnel junction are very special. The shaking table test should reproduce the features of this particular part of the shield tunnel authentically.

2 TEST DESIGN

2.1 *Similitude relations*

Constrained by testing conditions, shaking table tests on tunnels have always been performed on scaled models. The similitude relations in this paper are obtained through both the governing equation method and the Buckingham-π theorem. The derivation process could be found in the paper of Yan et al. (2015). Similitude ratios of geometry and acceleration could be predetermined according to conditions of the testing facilities. They are 1/60 and 4/1, respectively.

2.2 *Design of the model soil*

The prototype ground soil has a unit weight of 19.1 kN/m^3, a shear wave velocity of 243 m/s, and a maximum shear modulus of 115 MPa. Similitude ratios of the soil should fit the following equation:

$$S_a = \frac{S_G}{S_l S_\rho} \tag{1}$$

where S_a, S_G, S_I and S_ρ are similitude ratios of acceleration, shear modulus, geometry and density, respectively. The approach originally proposed by Shang et al. (2006) is adopted in this study. The synthetic model soil is composed of sawdust and sand, of which the mass ratio is 1:2.5. Maximum shear modulus of the synthetic soil is obtained via tri-axial test, which is 2.84 MPa. Density of the model soil is 694 kg/m^3. Given that S_I equals 1/60, the similitude ratio of acceleration calculated by equation (1) is 4.16, which is close to the predetermined value of 4. It should be noted that the gravity field is not adjusted to this similitude ratio, which is a common issue for scaled shaking table tests in geotechnical engineering. The relative-stiffness relation, considered as the controlling factor, might be affected by this. However, the influence is limited, and the requirement of similitude relations may be relaxed when considering the test results apart from the prototype system. The tri-axial test gives the relation of normalized shear modulus degradation with shear strain and the relation of damping ratio with shear strain. Comparison of the two relations between the synthetic soil and the ground soil is depicted in Figure 1. It is shown that they have similar dynamic properties. Therefore, the synthetic soil could work as the host medium in the scaled model test.

2.3 *Design of the tunnel model*

Individual tunnel ring models, called segmental equivalent rings, are designed to imitate the discontinuities in the shield-driven tunnel. Inner and outer diameters of the ring are 228 mm

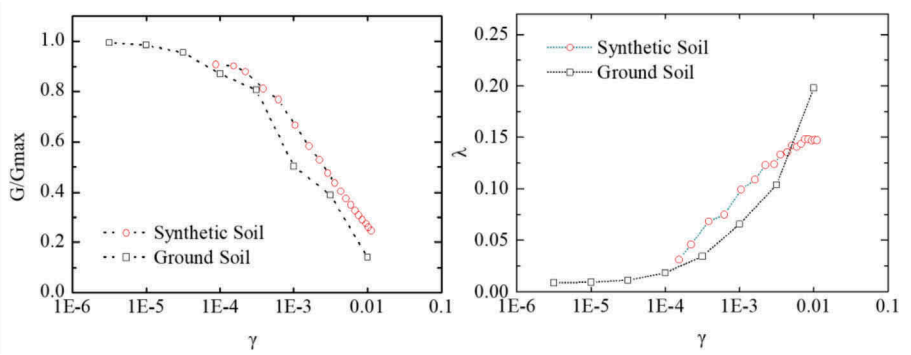

Figure 1. Comparison of dynamic properties between the synthetic soil and the ground soil.

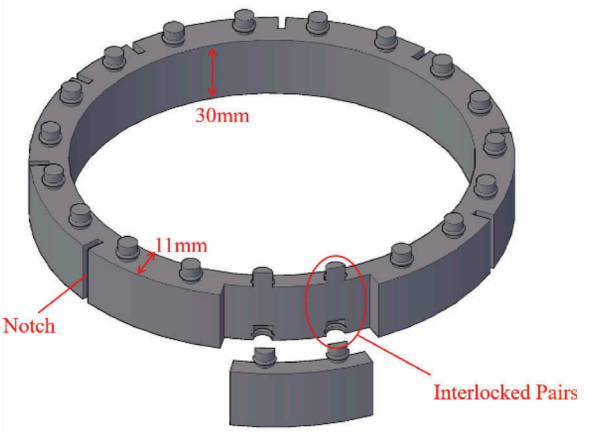

Figure 2. Segmental equivalent ring.

and 250 mm, respectively. Width of each ring is 30 mm along the longitudinal axis. As shown in Figure 2, there are 10 notches on the external surface of the ring model. The ring model is made of polyethylene. It has an elastic modulus of 0.79 GPa. Both the notches and the interlocked pairs are designed according to local properties of the ring. Their influence on the overall transverse and longitudinal stiffness of the tunnel model is validated through static test and numerical analysis (Bao et al. 2017).

2.4 *Design of the shaft model*

In previous studies, simplified shaft (station) models were designed comprising the major structural members only, for instance, enclosing walls, supporting beams, columns and slabs. (Saito et al. 2006; Chen et al. 2015; Chen et al. 2016; Ma et al. 2017) However, every elementary structure has its own contribution to the overall stiffness and mass distribution of the vertical shaft. It is reasonable to ignore some less important features of the prototype structure, but it surely is a better solution if the shaft model could be as realistic as possible. The advantage of 3D print technology over traditional manufacturing methods is that it enables designers to achieve all the desired details in the model with high precision. In this case, a scaled (by 1/60) digital replica of the vertical shaft is built as shown in Figure 3. It

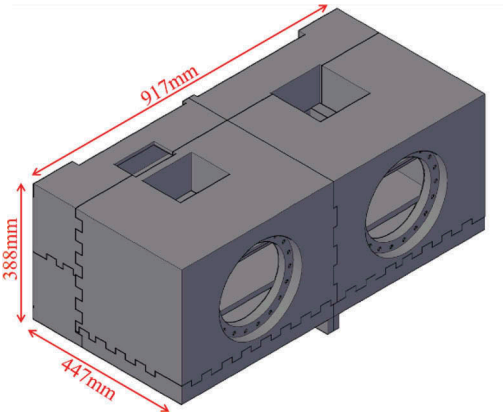

Figure 3. Digital replica of the vertical shaft.

has the same structural configurations as the prototype shaft, including minor components like inclined slabs, supporting caps on columns, tapered beams, walls with variable thickness, air openings, etc. The size of the shaft model shown in Figure 3 exceeds limits of most 3-D print machines, so the original model is partitioned into 8 pieces and printed separately. All the splitting surfaces are jagged, so different parts could be easily assembled and glued. The printing material is nylon. The density is 930 kg/m^3, and the elastic modulus is 1650 MPa.

2.5 *Instrumentation*

The shaft-tunnel model is placed at the longitudinal center line of the container box as shown in Figure 4. Distance between the shaft and the end plate is 2000 mm. The twin tunnel model is 6000 mm long. Depth of the model soil is 1400 mm. The shaft model is buried 385 mm beneath the soil surface. The monitored section of the shaft-tunnel model is marked in Figure 4. Sensors in this section are illustrated in Figure 5.

There are 7 uniaxial accelerometers from AW, A1 to A6 recording transverse acceleration re-sponses of the tunnel model. There is an accelerometer recording the acceleration response of the soil around the shaft-tunnel model, namely, AS1. Structural responses of the shaft-tunnel junction are revealed by the extension of circumferential joints. The extension of 8 circumferential joints is monitored as marked by JW and J1 to J7 in Figure 5. JW is the circumferential joint between the shaft model and the tunnel model.

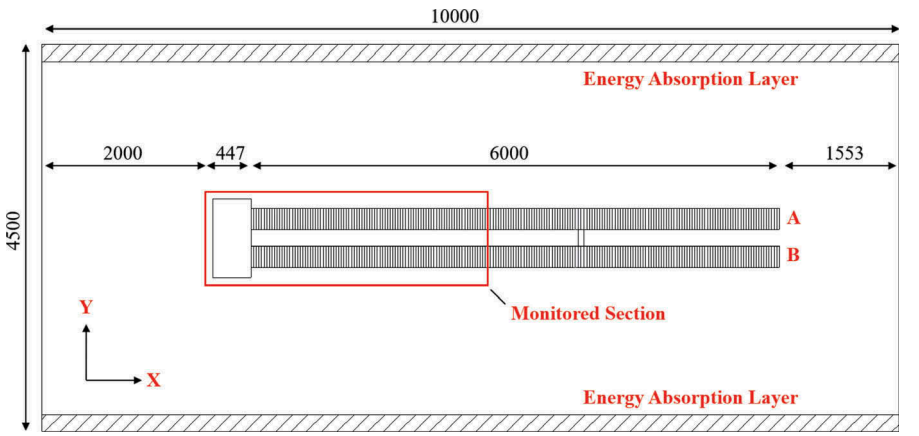

Figure 4. Schematics of the test. (unit: mm)

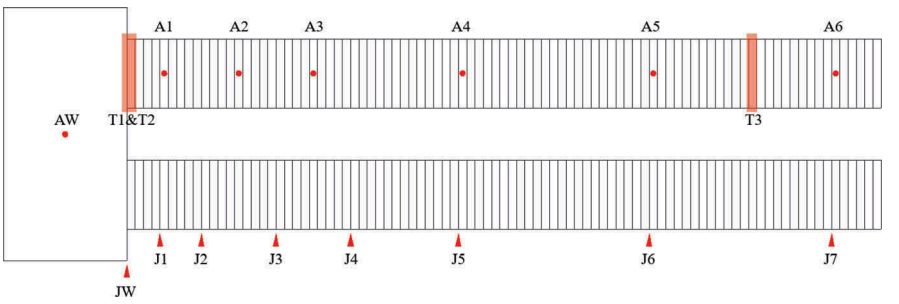

Figure 5. Sensors on the shaft-tunnel model.

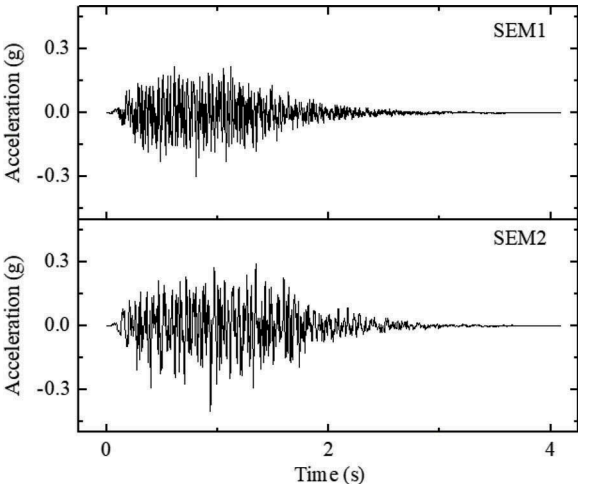

Figure 6. Time histories of the synthetic earthquake motions adopted in the test.

2.6 *Earthquake motions and testing cases*

Synthetic earthquake motions (SEM) are adopted as the input signals for the shaking table. Acceleration time histories of the synthetic earthquake motions are depicted in Figure 6. Notice that both the length and the amplitude of the acceleration time histories are scaled according to the similitude ratios. Shaking direction of the table is along the transverse direction of the tunnel model, i.e., along Y axis in Figure 4. In Case1, the input earthquake motion is SEM1. It has a peak acceleration of 0.30 g, and the dominant frequency is 26.6 Hz. In Case2, the input earthquake motion is SEM2. It has a peak acceleration of 0.40 g, and the dominant frequency is 23.9 Hz.

3 TEST RESULTS

3.1 *Acceleration responses of the shaft-tunnel model*

Acceleration data of the four accelerometers, AW, A4, A5 and A6, are roughly simultaneous, which is understandable because underground structures generally follow the ground movements during earthquakes. Spectral analysis is conducted. Acceleration spectra of AS1 are taken as the baseline to evaluate acceleration amplification of the other accelerometers. Divided by the amplitude of AS1, acceleration amplification spectra of AW, A4, A5 and A6 are shown in Figure 7. In both cases, most amplification factors of the four accelerometers are allocated near 1.0. Except in the range from 10 Hz to 30 Hz, the shaft model (AW) has significantly larger amplifi-cations indicted by the black peaks. Dominant frequencies of the input earthquake motions also fall in this range. Consequently, sensor AW has larger peak accelerations compared to the others. Peak accelerations of the 7 accelerometers from Case1 and Case2 are depicted in Figure 8. Sensor A1 and A2 are influenced by the shaft model, which gives the curves an increasing trend coming close to the shaft model from right to left. These are manifestations of the asynchronous acceleration responses between the shaft model and the tunnel model.

The curves in Figure 9 only presents 14 discrete data of the acceleration responses. The max-imum accelerations are recorded at different positions in different times. To statistically quantify the overall similarity of different acceleration time histories, correlation coefficients are calculated by the following equation:

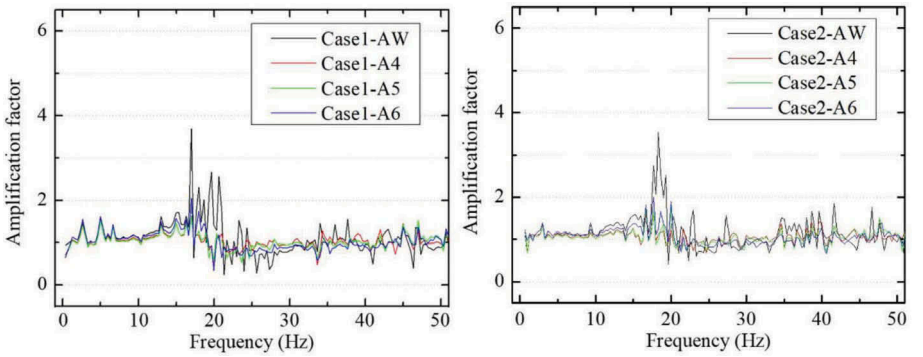

Figure 7. Acceleration amplification spectra of the shaft-tunnel junction.

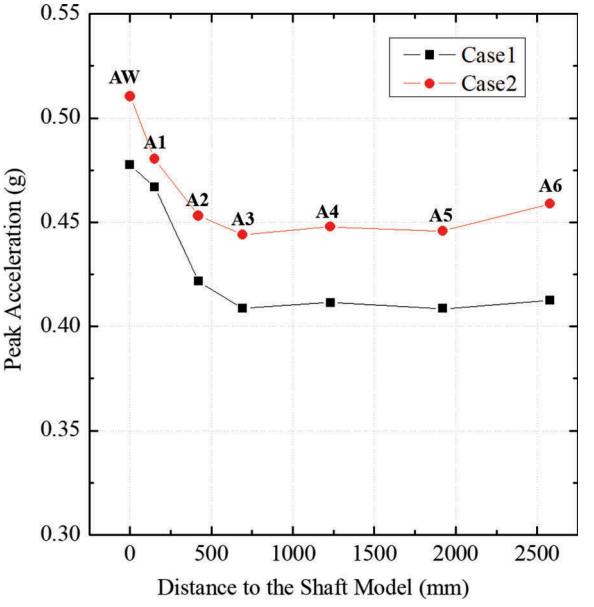

Figure 8. Peak accelerations of the shaft-tunnel model.

$$\rho_{nm} = \frac{\mathrm{cov}(A_n, A_m)}{\sqrt{D(A_n)D(A_m)}} \tag{2}$$

where A_n and A_m are acceleration time histories of accelerometer A(n) and A(m); ρ_{nm} is correlation coefficient of A_n and A_m; cov(A_n, A_m) is covariance of A_n and A_m; $D(A_n)$ and $D(A_m)$ are variances of A_n and A_m.

Correlation coefficients of the acceleration responses in Case1 and Case2 are calculated and shown in matrix form. For instance, the number at the second line and the third column is the correlation coefficient of the acceleration time histories of sensor A1 and A2. By definition, the matrixes are symmetric, and the elements of the main diagonal are 1.00.

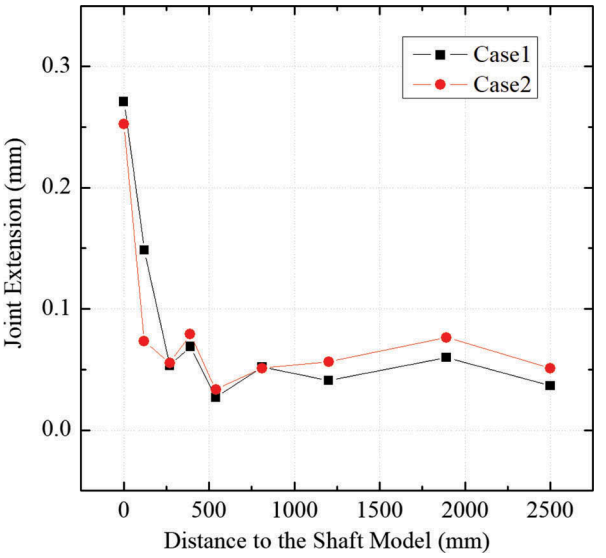

Figure 9. Maximum extensions of the circumferential joints.

Case1 :

	AW1	A1	A2	A3	A4	A5	A6	
AW1	1.00	0.96	0.88	0.83	0.79	0.80	0.79	AW1
A1	0.96	1.00	0.97	0.94	0.91	0.91	0.90	A1
A2	0.88	0.97	1.00	0.99	0.97	0.96	0.96	A2
A3	0.83	0.94	0.99	1.00	0.99	0.98	0.98	A3
A4	0.79	0.91	0.97	0.99	1.00	0.99	0.99	A4
A5	0.80	0.91	0.96	0.98	0.99	1.00	0.99	A5
A6	0.79	0.90	0.96	0.98	0.99	0.99	1.00	A6

Case2 :

	AW1	A1	A2	A3	A4	A5	A6	
AW1	1.00	0.97	0.90	0.85	0.81	0.82	0.83	AW1
A1	0.97	1.00	0.98	0.95	0.91	0.91	0.91	A1
A2	0.90	0.98	1.00	0.99	0.97	0.97	0.96	A2
A3	0.85	0.95	0.99	1.00	0.99	0.98	0.98	A3
A4	0.81	0.91	0.97	0.99	1.00	1.00	0.99	A4
A5	0.82	0.91	0.97	0.98	1.00	1.00	0.99	A5
A6	0.83	0.91	0.96	0.98	0.99	0.99	1.00	A6

All the correlation coefficients in the matrixes are positive and larger than 0.79. This means that the entire shaft-tunnel junction has similar acceleration responses because the shaft and the tunnel are driven by the same ground movements. Despite that, the five elements at the right of

the first line are the only ones less than or equal to 0.90 in both matrixes, while the correlation coefficients among A2, A3, A4, A5 and A6 are no less than 0.96. Sensor Al is affected by the shaft, so the elements in the second line decline from left to right gradually. The matrixes confirm the asynchronous responses at the shaft-tunnel junction. The influence of this discrepancy on structural performance is evaluated by extensions of circumferential joints in the longitudinal direction.

3.2 *Maximum extensions of circumferential joints*

The extension of the circumferential joints is one of the most concerned features in tunnel engineering. As illustrated in Figure 5, there are 8 circumferential joints monitored during the test. From the shaft model to the far end of the tunnel model, they are JW and J1 — J7. Maximum ex-tensions of the measured joints caused by the earthquake input in Case 1 and Case2 are plotted in Figure 9. The curves rise radically near the shaft model. Joint JW, which is the interface between the shaft model and the tunnel model, has the largest extensions in both cases. From JW to J3, the extension continues to decline. The joint extensions become stable with minor fluctuations after J4. Among the measured joints, J7 could be considered as a typical ordinary circumferential joint unaffected by the existence of the shaft. Compared to J7, the maximum extension of JW is raised by 642% and 396% in Case1 and Case2, respectively.

A major difference between the two input earthquake motions for Case1 and Case2 is their peak accelerations. Since SEM2 in Case2 is the stronger one, the curve of Case2 in Figure 8 is completely over the other one. Nevertheless, the two curves in Figure 9 are intertwined instead of one being above the other. This means that the absolute value of the structure's acceleration responses contributes little to the extension of circumferential joints. Meanwhile, the differences of peak accelerations between AW and A3 are 0.069 g in Case3 and 0.066 g in Case4. The matrixes of correlation coefficients also prove that the discrepancy between the shaft model and the tunnel model is quantitatively similar in the two cases. It is the asynchronous behaviors of the shaft and the tunnel that cause the circumferential joints to extend. Otherwise, if the shaft-tunnel junction could react in total synchronization, there would be no additional joint extension induced by the earthquake motions.

4 CONCLUSIONS

Shaking table test was conducted to study the asynchronous responses of the shaft-tunnel junction under transverse seismic impact. The following conclusions are drawn from the results.

The shaft-tunnel junction generally follows the behavior of surrounding soils, while they have special features of their own. The shaft model reacts more to the earthquake accelerations from 10 Hz to 30 Hz, which gives the curves of maximum accelerations a gradual declination from the shaft to the other end of the tunnel model. A more precise comparison of the shaft's and the tunnel's acceleration responses is shown by the matrixes of correlation coefficients. It offers a quantitative insight of the asynchronous responses of the shaft-tunnel junction.

The asynchronous acceleration responses have a significant influence on the extension of circumferential joints. The largest joint extension appears at the shaft-tunnel interface, where the structural change is most acute. The value of increment is directly related to the extent of dis-crepancy, not the absolute value, of the shaft's and the tunnel's acceleration responses.

REFERENCES

Bao, Z., Yuan, Y. & Yu, H. 2017. Multi-scale physical model of shield tunnels applied in shaking table test. Soil Dynamics and Earthquake Engineering100: 465–479.

Chen, G., Chen, S., Zuo, X., Du X., Qi, C. & Wang, Z. 2015. Shaking-table tests and numerical simulations on a subway structure in soft soil. Soil Dynamics and Earthquake Engineering 76: 13–28.

Chen, Z., Chen, W., Li, Y. & Yuan, Y. 2016. Shaking table test of a multi-story subway station under pulse-like ground motions. Soil Dynamics and Earthquake Engineering 82: 111–122.

Kiureghian, A.D. 1996. A coherency model for spatially varying ground motions. Earthquake Engineering and Structural Dynamics 25(1): 99–111.

Koizumi, A. 2009. Seismic damages and case study for shield tunnel. Beijing: China Architecture and Building Press.

Ma, X., Wang, G., Wu, J. & Ji, Q. 2017. Experimental study on the Seismic Responses of Subway Station in Soft Ground. Journal of Earthquake and Tsunami 11(1): 1750020.

Saito, K., Yamane, K. & Koizumi, A. 2006. A Study on Seismic Behavior of Shield Tunnel Including Shaft in Longitudinal Direction. Journal of Tunnel Engineering, JSCE 16: 121–132.

Shang, S., Liu, F., LuH. & DuY. 2006. Design and experimental study of a model soil used for shaking table test. Earthquake Engineering and Engineering Vibration 26(4): 199–204.

Yan, X., Yu, H., YuanY. & YuanJ. 2015. Multi-point shaking table test of the free field under non-uniform earthquake excitation. Soils and Foundations 55(5): 985–100.